Ann. Occup. Hyg., Vol. 57, No. 2, pp. 184–199, 2013

doi:10.1093/annhyg/mes063

Uncertainty in Aspiration Efficiency Estimates from Torso Simplifications in Computational Fluid Dynamics Simulations

KIMBERLY R. ANDERSON and T. RENÉE ANTHONY*

Department of Occupational and Environmental Health, University of Iowa, 105 River Street, CPHB S333, Iowa City, IA 52242-5000, USA

Received 19 March 2012; in final form 13 July 2012; published online 21 September 2012

Computational fluid dynamics (CFD) has been used to report particle inhalability in low velocity freestreams, where realistic faces but simplified, truncated, and cylindrical human torsos were used. When compared to wind tunnel velocity studies, the truncated models were found to underestimate the air's upward velocity near the humans, raising questions about aspiration estimation. This work compares aspiration efficiencies for particles ranging from 7 to 116 µm using three torso geometries: (i) a simplified truncated cylinder, (ii) a non-truncated cylinder, and (iii) an anthropometrically realistic humanoid body. The primary aim of this work is to (i) quantify the errors introduced by using a simplified geometry and (ii) determine the required level of detail to adequately represent a human form in CFD studies of aspiration efficiency. Fluid simulations used the standard k-epsilon turbulence models, with freestream velocities at 0.1, 0.2, and 0.4 m s^{-1} and breathing velocities at 1.81 and 12.11 m s^{-1} to represent at-rest and heavy breathing rates, respectively. Laminar particle trajectory simulations were used to determine the upstream area, also known as the critical area, where particles would be inhaled. These areas were used to compute aspiration efficiencies for facing the wind. Significant differences were found in both vertical velocity estimates and the location of the critical area between the three models. However, differences in aspiration efficiencies between the three forms were <8.8% over all particle sizes, indicating that there is little difference in aspiration efficiency between torso models.

Keywords: aerosols; computational fluid dynamics; dust sampling conventions; inhalable dust

INTRODUCTION

The use of torso simplification in wind tunnel experiments and computer simulations investigating contaminant transport is common. Typical simplifications include truncation of a full-size mannequin at the waist or hip to allow height reduction of experimental wind tunnels. In computational fluid dynamics (CFD) studies, torsos have been simplified by using geometrical surrogates, including cylindrical and block forms (e.g. Brohus and Nielsen, 1996), as well as truncation at hip or waist heights. However, the effect of using simplified geometries as surrogates for realistic human features has not been thoroughly investigated, particularly in particle aspiration studies with constant or cyclical inhalation through the mouth or nose.

Most aspiration studies have used torso simplifications, although the degree of simplification can vary dramatically from study to study. The initial experimental aspiration studies by Ogden and Birkett (1975) simply used an isolated head, but later studies included representations of the torso to better reflect how air upstream of the body decreases streamwise and increases laterally and vertically to move

*Author to whom correspondence should be addressed.
Tel: +319-335-4429; fax: +319-384-4138;
email: renee-anthony@uiowa.edu

around the torso. To allow for reasonable wind tunnel heights, Aitken *et al*. (1999), Kennedy and Hinds (2002), and Maynard *et al*. (1997) used mannequins with the torso truncated at the waist in inhalability experiments. Early numerical studies investigating aspiration evaluated a two-dimensional cylindrical sampling head (Ingham, 1981), although later computational studies have included realistic facial features with cylindrical truncated torso (Anthony, Flynn and Eisner, 2005) and full-sized, realistic human models (Se *et al*., 2010). Although commonly used, the effects of airflow patterns, particle transport, and particle aspiration using the truncated torso simplification have not been explicitly investigated.

In order to adequately assess aspiration efficiency in computational studies, research needs to determine the level of complexity required in torso geometries. Thermal studies investigating airflow and pollution transport around human bodies have more extensively investigated the impact of torso simplifications on airflow and contaminant transport. Although these studies lack breathing (inhalation or exhalation), they have identified that torso complexity can influence airflow around the body and, more importantly, within the facial region. Murakami *et al*. (2000) shows that as warm air rises around a human body, the airflow accelerates vertically as it passes from the neck to the head region. Topp *et al*. (2003) illustrates that the presence of legs causes a decrease in velocity at the center of the torso compared to a torso with no legs. These studies would indicate that neglecting legs in a model could cause an increase in aspiration efficiency due to the increased upward velocity at the center of the chest.

Studies examining the effect of torso geometry on sampler aspiration efficiency have also contributed to our understanding of airflow around the human body. One study found that the use of a simplified torso (fashioned from a wastebasket) resulted in aspiration efficiencies 35% that of the samplers placed on a human-shaped mannequin with torso truncation (Kennedy *et al*., 2001). Sampler studies conducted by Smith and Bird (2002) identified a decrease in vertical velocity in the chest region, with a smaller decrease in the facial region using a full-sized, tailor's mannequin, again truncated at the waist. However, like the thermal studies, these investigations lacked inhalation at the mouth, so the influence of these flow differences near an inhaling mannequin is unknown.

Anthony *et al*. (2005) compared airflow around a small-scale inhaling anatomical mannequin to that of a finite elliptical torso in a wind tunnel study. They identified significant velocity differences in the facial region and attributed this to facial feature differences, recommending future simulations including realistic facial features from the neck up, at a minimum. Anthony and Flynn (2006a) compared airflow and particle transport between wind tunnel and CFD simulation experiments, where the simulations used a humanoid geometry that matched their 2005 test mannequin's facial features but simplified the torso with an elliptical cylinder truncated at hip height. They could not resolve the effects of velocity differences between simulation and experimental data by repositioning the simulated particle source within 5 mm of the matched experimental position, indicating that torso simplification resulted in velocity differences sufficient to shift the critical upstream aspiration area. In later full-scale human simulations, Anthony and Flynn (2006b) compared computational aspiration efficiencies to facing-the-wind experimental data from Kennedy and Hinds (2002). Particles smaller than 52 µm compared well with the experimental results from Kennedy and Hinds (2002), but for particles larger than 52 µm the CFD model underestimates aspiration efficiencies compared to published results. Anthony and Flynn hypothesized that the truncated, simplified torso in the CFD model may have contributed to velocity differences that may have affected aspiration efficiency estimates.

Simplifications to the human torso, including truncation at hip/waist height or ignoring leg separation, could have two effects. By placing a solid horizontal surface at the hip height, zero upward velocity is established at the hip height, not representative of airflow around a full-height humanoid. By using a solid torso that ignores the separation of legs, the streamwise velocity would be smaller and the vertical velocity would be larger in the region where legs would really exist, where air is allowed to pass between rather than forced to turn upward and laterally to move around the bluff body. These differences may be more important in indoor workplaces where velocities are relatively small, because particle transport would be more influenced by the personal climate around the body, than the freestream velocities.

Hence, experiments were needed to improve our understanding of the relationship between torso simplifications and their effect on the velocity field, particle trajectories within these affected fields, and, ultimately, aspiration efficiency estimates.

This study explicitly examines the effects of using simplified torso geometry on estimates of large particle aspiration efficiency. Three torso geometries were evaluated to compare velocity and aspiration estimates between both a simple geometry (elliptical

torso matching the 50th percentile female height) and a truncated simple geometry compared to the baseline of a realistic model with legs, arms, and torso matching the same 50th percentile female dimensions. The study examines whether the torso height and shape affects (i) the velocity field near the mouth, (ii) the position of upstream critical areas that result in aspirated particles, and (iii) the estimates of aspiration efficiency. Objective 1 explores how much the upstream velocity changes based on the torso shape with an inhaling mouth. Objective 2, while necessary to generate the data to evaluate the third question, also allows for the examination of whether simplified torsos are sufficient to model contaminant transport 'from a source.' Although not critical to aspiration efficiency estimates, the position of the critical area is useful to understand the limitations of simplified CFD or wind tunnel mannequins in exposure assessment applications where contaminants are generated from a fixed position within the environment. Objective 3 examines whether differences identified in contaminant transport result in different estimates of aspiration efficiency.

METHODS

Geometry description

Three torso geometries were generated (Gambit, Ansys, Inc., Lebanon, NH, USA) to investigate the effects of simplification on particle aspiration: a simplified cylindrical torso truncated at hip height, a full-height simplified cylindrical torso, and an anatomical torso with realistic dimensions and arms and legs (Fig. 1). All the three humanoid forms used identical head and neck geometries, based on the small nose, large lips, and rounded rectangular mouth inlet (area = 6.9496×10^{-5} m^2), fully described in Anthony (2010). The first geometry ('Truncated') used an elliptical torso—0.2775 m tall, 0.2325 m wide, and 0.1725 m deep—representing truncation at hip height. This geometry was identical to that used in previous work (Anthony and Flynn, 2006b, which used a different solver [FIDAP]) to compare aspiration performances between geometries. The second geometry ('Full') extended the elliptical torso to a height of 1.07 m, for a total humanoid height of 1.56 m, approximating the 50th percentile female height. The final geometry ('Anatomical') incorporated a realistic anatomical human torso that matched the height of the second geometry and approximated the 50th percentile female dimensions in other dimensions (Table 1). The hands and feet were simplified by truncation, assuming that their influence on simulations of particle trajectories into an inhaling mouth would be negligible.

To evaluate whether the influence of torso simplification resulted in differences between previous simulations (Anthony and Flynn, 2006b) and experimental work (Kennedy and Hinds, 2002), this study focused on facing-the-wind orientation. The conditions were selected to match those

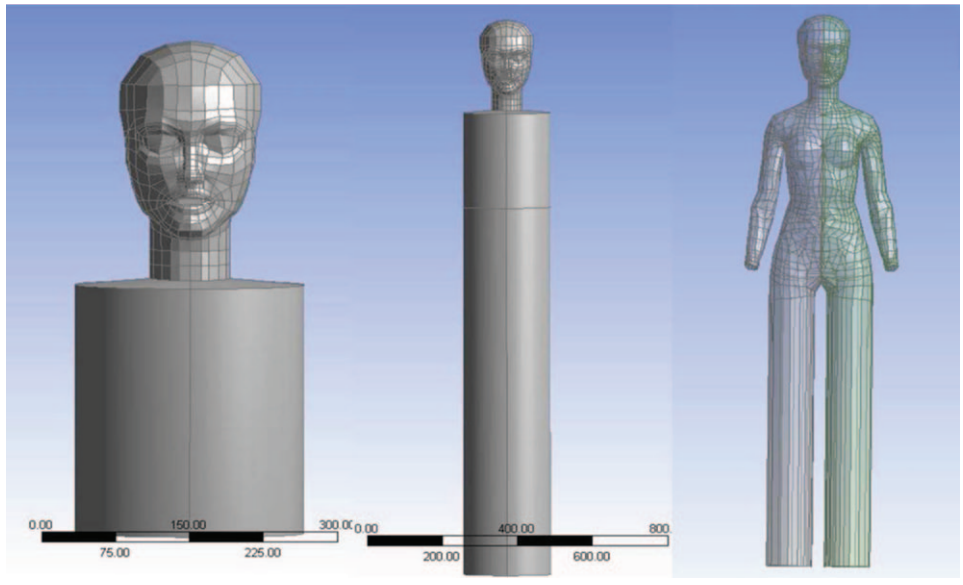

Fig. 1. Illustrations of truncated, full, and anatomical geometries (left to right).

Table 1. Comparison of dimensions between the anatomical model and the 50th percentile female dimensions.

Surface	Anatomical geometry dimension (m)	50th Percentile female dimensions	Difference (%)
Height	1.56	1.625	1.04
Shoulder height	1.34	1.325	0.99
Elbow height	1.11	1.02	0.91
Hip height	0.99	0.835	0.84
Knee height	0.67	0.505	0.75
Width at temple	0.086	0.072	1.19
Chin to top of head	0.19	0.218	0.87
Center of mouth to top of head	0.154	0.178	0.86
Forehead to back of head	0.155	0.18	0.86

of Kennedy and Hinds (2002), which are the only experimental orientation-specific data available in low velocities. Facing-the-wind orientation allowed the assumption of lateral symmetry, which required only the left half of the torso and the computational domain to be simulated, thereby reducing the computational time.

Each of these humanoid forms was positioned within a computation domain to simulate a wind tunnel (Fig. 2). The mouth opening was fixed at the origin for all geometries tested, and the inlet wall was positioned 1.8525 m in front and the outlet wall was 1.8051 m behind the mouth center. The width of the computational domain was 1.142 m for each form. For the full-height geometries, the domain extended 2.3 m from floor to ceiling, but was reduced to 1.23 m for the truncated domain, where the base of the truncated torso coincided with the floor height. These dimensions were chosen so that the geometries were located far enough away from these planes so that (1) the flow upstream of the humanoid forms would be fully developed (distance > 4 diameters), (2) the assumption of no acceleration through the outflow of the domain was reasonable (distance > 10 diameters), and (3) the fluid field was not influenced by the location of the side and top walls (blockage ratio was ~11%).

Mesh generation and refinement

Ansys 12.0 (Ansys, Inc, Lebanon, NH, USA) was used to mesh the computational domain. A paved meshing scheme was used because of the complex geometries involved, using triangular surface and tetrahedral volumetric elements. To evaluate the quality of the simulations' solutions, three sequential mesh refinements were generated for each geometry by

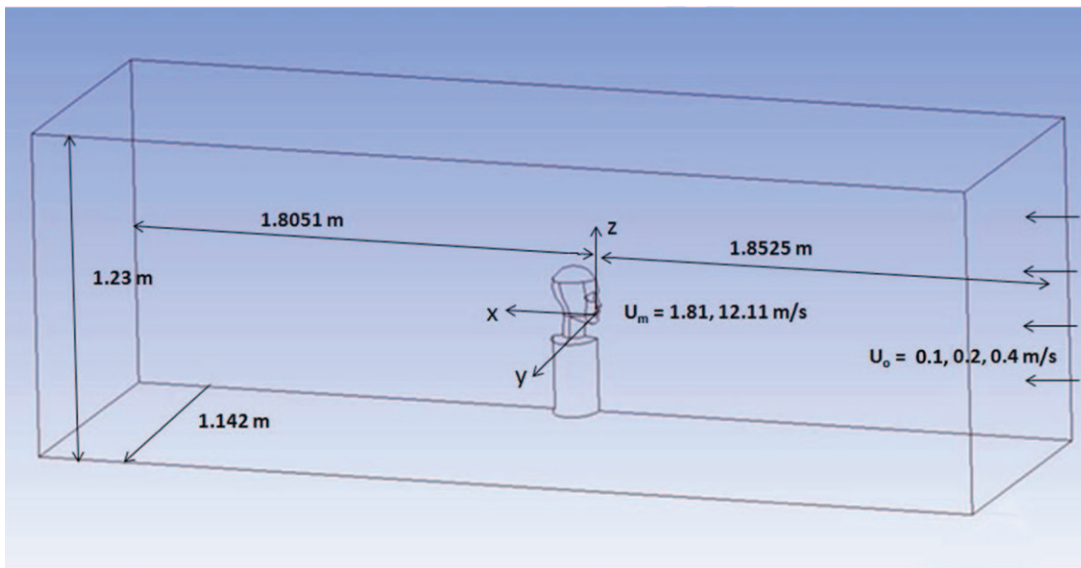

Fig. 2. Computational domain dimensions and orientation (truncated model shown).

increasing the node counts on each edge by a factor of 1.2. When mesh convergence was not achieved, a second set of three-mesh densities were created, using the moderate and fine meshes and generating a new mesh density between these two. To create this moderate-fine mesh density, the node count of the moderate mesh was increased by a factor of 1.1.

Mesh-refinement factors were computed from the total number of nodes used between sequential meshes $\left(\sqrt[3]{N_{\text{refined}}/N_{\text{coarser}}}\right)$ within a geometry, and ranged between 1.208 and 1.287 for the coarse-moderate-fine three-mesh series. Using the three-mesh series that excluded the coarse mesh and examined a mesh between the moderate and fine mesh densities, mesh refinement factors ranged from 1.097 to 1.107. The node counts ranged from 300 000 to 700 000 for coarse meshes and 1.1 to 2.3 million for the refined meshes, with more complex geometries requiring more nodes to discretize the surfaces and volume. For the most refined mesh, the average spacing between nodes within the domain was 17 mm with smaller distances near the humanoid surface. The average spacing of nodes around the mouth edge was 0.477 mm, again for the most refined mesh. Additional details of the mesh refinement and the number of elements and nodes for each torso geometry are shown in the Supplementary data available at *Annals of Occupational Hygiene* online.

Computational method

All simulations were conducted on 64-bit processor personal computers with 8–12 GB RAM using the Windows XP operating system. Fluent 12.0 (Ansys Inc, Lebanon, NH) was used to solve the fluid flow field before conducting particle simulations. For this work, six degrees of freedom were investigated: three velocity components (streamwise = U, lateral = V, vertical = W), turbulence kinetic energy (KE), dissipation of turbulence kinetic energy (E), and pressure (P).

The airflow was modeled using steady-state, incompressible, turbulent, Navier–Stokes equations (detailed in the Supplementary data available at *Annals of Occupational Hygiene* online).

Full buoyancy effects were modeled. Gravity was set to act downward at 9.81 m s^{-2}. Indoor room air temperature was simulated (20°C) with the corresponding air density (1.205 kg m^{-3}) and viscosity (1.83692×10^{-5} kg m^{-1} s^{-1}).

Two breathing rates at three freestream velocites were investigated. A uniform velocity of 0.1, 0.2, or 0.4 m s^{-1} was assigned to the domain entrance, to represent a range of low-velocity indoor air conditions typical of workplaces (Baldwin and Maynard, 1998). The experimental work by Kennedy and Hinds (2002) only investigated wind speeds at 0.4 m s^{-1}, so comparisons to experimental work could not be made for the 0.2 or 0.1 m s^{-1} velocity conditions. Two constant inhalation velocities were assigned to the rounded-rectangular mouth surface, chosen to represent at-rest (1.81 m s^{-1}) and heavy (12.11 m s^{-1}) breathing. These are mathematically equivalent to the mean inhalation velocities for 7.5 and 50.3 l min^{-1} cyclical breathing rates and allow for an examination of aspiration differences over a range of likely inhalation velocities at the mouth.

Other boundary conditions applied included standard wall function at all solid surfaces, where velocity and turbulence parameters were set to zero. The bottom of the computational domain (the 'floor') for full-height geometries were also assigned as walls. However, the 'floor' for the truncated geometry was assigned as a symmetry plane, which allowed air to move along this surface but not through it. This assignment forced zero vertical velocity in this transverse plane, which was the same simplification used in the previous work. This truncation and the boundary condition were expected to result in an underestimate of vertical velocity throughout the domain, compared to the taller geometries. However, examination of whether this affected particle trajectories and, ultimately, aspiration efficiency, was an explicit outcome evaluated in this study. All other unassigned nodes were assigned initial velocities equivalent to the freestream velocity (0.1, 0.2, or 0.4 m s^{-1}), according to the simulation underway.

For all tests, an 8% turbulent intensity and a ratio of eddy to laminar viscosity of 10, typical of wind tunnel studies, were assigned to the domain entrance and as initial conditions to all unassigned nodes throughout the domain.

Solutions were obtained using the SIMPLE algorithm, with second-order upwinding, when the global solution errors (GSE) reached predetermined tolerances of 10^{-3}, 10^{-4}, and 10^{-5}. At each of these levels, estimates for each of the six degrees of freedom were extracted from the solved flow field and were evaluated to examine iterative convergence and mesh independence over 1710 positions. These locations were selected from upstream positions (X) from −0.015 to −0.75 m, lateral positions (Y) from 0 to 0.75 m, and vertical positions (Z) from −0.3 to 0.6 m. Details of solution verification are described in the Supplementary data available at *Annals of Occupational Hygiene* online. In short, non-linear convergence tests examined L_2 error norms, with an

a priori target of less than 5%, and mesh independence was examined using the three-mesh R_2 error norms, with targets below 1.0.

Particle release and tracking

Once the quality of the fluid field estimates was evaluated, particle simulations were performed to estimate aspiration efficiencies for each geometry and velocity condition. The Euler–Lagrange approach was used to solve for particle motion. Laminar particle trajectories were examined; thus, the estimates of aspiration efficiency reflect mean values and cannot incorporate uncertainty due to turbulent particle behavior. Particle momentum equations and spherical drag law are described fully in Anthony (2010).

The particle trajectories of seven aerodynamic particle sizes were examined (7, 22, 52, 68, 82, 100, and 116 µm). These particle sizes were chosen to match experimental data from Kennedy and Hinds (2002) and simulations of Anthony and Flynn (2006b).

Non-evaporating, unit-density particles were released, which allowed for reporting in aerodynamic diameters. The release points were located more than four head diameters away from the torso models to ensure that the freestream was not affected by the downstream bluff body (Chung and Dunn–Rankin, 1997). As such, the particles were released 0.75 m upstream of the mouth opening for particles smaller than 82 µm. At larger sizes, gravitational settling contributes significantly to a particle's trajectory in low velocity air. As the particle size increased, upstream particle releases at X = 0.75 m required releases near and above the top of the computational domain, where the boundary layer at the top wall of the domain could affect the velocity field. Hence, for particles 82 µm and larger, release positions were moved closer (X = 0.4 m upstream of the mouth opening). For these particles, release positions were sufficiently upstream and above the head so that bluff-body effects in this region were negligible (no reduced velocity from torso blockage, no increased velocity from acceleration over the head, and no lateral or vertical turning to go around the head).

To meet the uniform particle distribution assumption, particles were released at velocities that incorporated the freestream velocity at the release location and the particle's terminal settling velocity. This was accomplished by assigning a horizontal velocity equal to the velocity in the wind tunnel at the release position and a vertical velocity equal to the combination of the initial velocity of the freestream at the release location combined with a downward component equal to the terminal settling velocity of the particle being evaluated.

Determination of critical area

Particle simulations were performed to identify the upstream positions and the cross-sectional area where particles would travel from the freestream and terminate in the mouth, thereby being inhaled. The upstream area containing all release positions that result in particle inhalation is defined as the critical area. These positions were identified by stepping through a series of lateral (Y) positions ($\triangle Y$ = 0.005 m) and releasing 100 particles along a 10-mm vertical line ($\triangle Z$ = 0.0001 m) to determine the minimum and maximum heights corresponding to an inhaled particle at a given lateral position. The maximum and minimum heights (Z-coordinates) across the lateral (Y) positions defined the location of the critical area. The critical area was computed, as detailed in Anthony and Flynn (2006b), and the midpoint of this area was also computed to compare positions of critical areas between torso geometries.

Once the critical area was identified for a set of test conditions and geometries, the aspiration efficiency fraction was computed using equation 1 (Anthony and Flynn 2006b):

$$\text{Aspiration Efficiency}, \% = \frac{A_c U_c}{(A_m U_m)} \quad 100\% \qquad (1)$$

where

A_c =Critical area, defined as the upstream area where particles are aspirated into the mouth, m^2
U_c =Freestream velocity within this critical area, m s^{-1}
A_m =Mouth-opening area, m^2
U_m =Velocity through the mouth opening, m s^{-1}

For each particle size (7) and velocity condition (6), 42 critical area positions and aspiration estimates were computed for each of the three human geometries studied.

Data analysis

Three sets of data were evaluated to examine the effect of geometry simplifications on estimates of aspiration efficiency. A reasonable hypothesis is that the truncation or shape of the torso would affect the vertical velocity within the region of the mouth. The first objective was to determine if vertical velocity in the chest and the facial region differed by geometry. If vertical velocities differed, this could shift the position of the upstream critical area that contained the stream of particles terminating in the mouth orifice. Hence, the second objective of this study was to compare the positions of the critical areas between geometries. Finally, even if the vertical velocities

differed and the position of the critical areas differed between geometries, then the third objective was to determine whether these differences would significantly affect the estimate of aspiration efficiencies over the range of test velocities and inhalable particle sizes evaluated.

To meet these objectives, estimates of vertical velocity, the center position of the critical areas, and resulting aspiration efficiencies were compared between the geometry types after evaluating the quality of the fluid flow estimates from each of the 12 test conditions. Vertical velocities were compared, matching by test velocities, to determine whether the torso shape affected the velocity field upstream of the humanoid mouth. The range and the average differences, between each geometry combination, were assessed. Paired *t*-tests (two-tailed) were performed to test whether, over matched conditions and locations, the estimates of vertical velocity significantly differed among test geometry.

Similarly, estimates of the midpoint for each critical area were determined and evaluated, by particle size and velocity condition, to determine whether the location of the critical area was statistically lower for more realistic geometries (paired, one-tailed *t*-test). Finally, aspiration efficiency estimates, matched by velocities and particle size, were evaluated to determine whether significant differences could be attributed to torso geometry (two-tailed, paired *t*-tests). These evaluations allowed the determination of whether the torso truncation or shape affected vertical velocity, critical area position, or, most importantly for the work at hand, aspiration efficiency.

RESULTS

Fluid simulations

For all geometries investigated, the coarse mesh took less than 1 day to achieve the solutions with GSE $< 10^{-5}$. The most refined meshes took up to 9 days to reach the solutions with GSE $< 10^{-5}$. The heavy breathing conditions for all geometries required more iterations to solve and had the most difficulty converging. The heavy breathing conditions were also more likely to not reach convergence at 10^{-5} level for the coarse mesh, requiring the additional mesh to be generated. The realistic humanoid form took longer to converge for all mesh densities, but the full model and the truncated model had similar convergence times.

Before particle simulations began, non-linear convergence and mesh independence studies were performed. Resulting L_2 error norm and three-mesh R_2 values are provided in full in Supplementary data available at *Annals of Occupational Hygiene* online. In brief, the at-rest breathing conditions solved well, whereas convergence problems with the heavy breathing condition were identified. For the L_2 error norm, for nearly all the freestream and breathing velocity conditions between the 10^{-4} and 10^{-5} solutions, the solution changed less than 5%, meeting the *a priori* criterion. The exception was for vertical velocity (W), turbulence kinetic energy (KE), and the dissipation of turbulent kinetic energy (E) at the 0.2 m s^{-1}, at-rest breathing condition for the full model. For between-mesh R_2 error norms, the anatomical and truncated torso models for at-rest breathing were well converged, except for KE at 0.4 m s^{-1} freestream. Heavy breathing for these same geometries demonstrated convergence for only two or three of the six degrees of freedom. The upward velocity (W) tended to not demonstrate monotonic convergence at the 10^{-5} GSE tolerance. In general, the at-rest breathing rate conditions showed monotonic convergence for more degrees of freedom than the heavy breathing rates. Although convergence was not confirmed for all mesh densities, increasing the mesh density tended to increase the number of degrees of freedom that demonstrated convergence, indicating that further mesh refinements should yield converged solutions. However, the mesh densities used in the most refined mesh were at the computational limit of the 12 GB RAM computers used in this simulation.

The least-refined mesh that indicated mesh independence was used for velocity extraction and particle simulations. For cases where mesh independence was not shown, the most-refined mesh density solution was used. For degrees of freedom that did not show mesh independence, it must be assumed that an additional mesh refinement would yield mesh independence for the following particle simulations to be valid.

Velocity estimates

Illustrations of the streamlines at the midsagittal plane for the 0.2 m s^{-1} freestream and heavy breathing rate, for each torso geometry, are provided in Fig. 3. Table 2 summarizes the range and average vertical velocity differences between the three torso geometries over the same 1710 upstream positions used for convergence studies, matched by freestream and breathing velocity simulations. Vertical velocities for the anatomical geometry were on average 0.002 m s^{-1} larger than the full model and 0.007 m s^{-1} larger than the truncated geometry. The vertical velocity for the full model was on average 0.005 m s^{-1} larger than the truncated geometry. The vertical

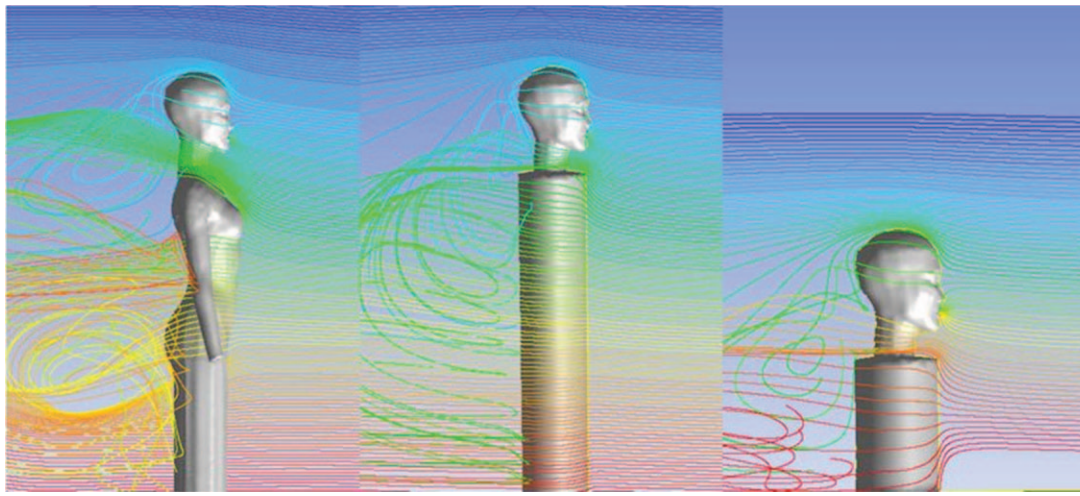

Fig. 3. Velocity streamlines around humanoids. Freestream velocity 0.2 m s^{-1} and heavy (12.11 m s^{-1}) breathing rate.

Table 2. Summary of differences between torso models.

	Vertical velocity (m s^{-1})			Critical area midpoint (mm)			Aspiration efficiency (%)		
	Min	Max	Avg	Min	Max	Avg	Min	Max	Avg
Anatomical-full	−0.21	0.29	0.002	−18	−3.2	−10.7	−10.9	7.2	0.7
Anatomical-truncated	−0.18	0.28	0.007	−36	−14	−23.8	−10.7	8.8	0.4
Full-truncated	−0.07	0.13	0.005	−17	−8.3	−13.1	−6.4	2.3	−0.3

velocity was significantly different between geometries over the entire region. Differences in vertical velocity between torso models were larger at the 0.4 m s^{-1} freestream velocity (0.006–0.016 m s^{-1}) compared to freestream velocities 0.2 m s^{-1} or less (0–0.009 m s^{-1}).

To examine where the velocity differences were more apparent, the velocity data were segregated into different regions: face region, defined as positions located just below the chin and upward ($Z = -0.05$ m to $Z = 0.6$ m), and the neck/chest region, including all positions below the chin ($Z = -0.05$ m to $Z = -0.3$). Vertical velocity estimates were paired between torso geometry, by freestream velocity, breathing rate, and location. Paired, two-tailed *t*-tests showed significant differences ($P < 0.001$) between the anatomical and full geometry velocities for all breathing rates and velocity conditions in both regions, except for between the anatomical and full models at 0.4 m s^{-1}, at-rest breathing rate ($P = 0.17$) in the below-the-neck region shown in Table 3. For vertical velocity data in regions above the neck, the trend of larger differences between torso models at the 0.4 m s^{-1} freestream velocity compared to the lower freesteam velocities was seen; but for regions below the neck, the differences between torso models was similar, regardless of the freestream velocity.

Over the range of at-rest and heavy breathing velocities and three levels of freestream velocity conditions, the hypothesized vertical velocity differences were confirmed between torso geometries. The impact of velocity differences on particle aspiration requires an investigation of how these differences affect the position of the stream-tube-containing particles that travel from the freestream to the inhaling mouth, namely by examining the position of upstream critical areas. Although velocity difference was statistically significant between torso geometries, these differences are smaller than many experimental measurement techniques could identify.

Critical area

Critical areas ranged from 2.87 to 41.30 cm^2 for the 7 µm particles, with larger areas associated with heavy breathing rates. As the particle size increased, the critical areas reduced to 0 to 10.73 cm^2 for the 116 µm particles tested, with no particles being inhaled at the low freestream, at-rest suction conditions. The location of the critical areas decreased in height above the mouth with increasing freestream velocity, for all

Table 3. Vertical velocity; minimum and maximum values by region. All velocities in m s^{-1}.

		Torso geometry								
		Anatomical			Full			Truncated		
Velocity	Breathing velocity	Min velocity	Max velocity	Average velocity	Min velocity	Max velocity	Average velocity	Min velocity	Max velocity	Average velocity
0.1	1.81	−0.010	0.052	0.009	−0.018	0.053	0.007	−0.024	0.047	0.005
0.1	12.11	−0.084	0.081	0.009	−0.01	0.052	0.009	−0.085	0.081	0.004
0.2	1.81	−0.002	0.104	0.018	−0.016	0.107	0.014	−0.057	0.094	0.009
0.2	12.11	−0.08	0.098	0.018	−0.105	0.098	0.014	−0.091	0.11	0.009
0.4	1.81	0.001	0.201	0.034	−0.043	0.22	0.028	−0.091	0.192	0.019
0.4	12.11	−0.075	0.205	0.034	−0.11	0.233	0.028	−0.098	0.208	0.018
0.1	1.81	−0.01	0.052	0.007	−0.018	0.049	0.005	−0.017	0.047	0.005
0.1	12.11	−0.084	0.046	0.006	−0.010	0.052	0.007	−0.085	0.040	0.003
0.2	1.81	−0.002	0.104	0.022	−0.016	0.107	0.018	−0.057	0.094	0.012
0.2	12.11	−0.08	0.098	0.022	−0.105	0.098	0.018	−0.091	0.11	0.011
0.4	1.81	0.001	0.201	0.042	−0.043	0.22	0.035	−0.091	0.192	0.024
0.4	12.11	−0.075	0.205	0.042	−0.11	0.233	0.035	−0.098	0.208	0.023
0.1	1.81	0.001	0.046	0.014	0.001	0.053	0.011	−0.024	0.047	0.005
0.1	12.11	0.001	0.081	0.017	0.001	0.046	0.014	−0.023	0.081	0.008
0.2	1.81	0	0.009	0.004	−0.001	0.021	0.004	−0.001	0.005	0.002
0.2	12.11	0	0.009	0.004	−0.001	0.009	0.002	−0.001	0.005	0.002
0.4	1.81	0	0.017	0.008	−0.001	0.012	0.005	−0.001	0.01	0.004
0.4	12.11	0	0.016	0.007	−0.001	0.011	0.005	−0.001	0.01	0.004

particle sizes and breathing rates. The between-torso differences in location of the critical area midpoint were greater as particle size increased. Differences between the midpoints of the critical area increased with decreasing freestream velocity for all torso geometries. Figure 4 illustrates the shape and the position of one set of critical areas (7 µm particles at 0.4 m s^{-1} freestream, at-rest breathing). Plotted is one-half of the critical area (only the $+Y$ half of the humanoid forms were simulated). The notch near the center top of the critical area was again identified in this work, reported by others as the reduction in critical area associated with particle impacting the lip and nose. The notch was slightly larger (0.072%) for the truncated torso simulations compared to the anatomical simulations. The difference in area due to the notch, however, is a small proportion (0.26% for the truncated model, 0.19% for the anatomical model) of the overall critical area that these differences may be negligible.

Coordinates defining these critical areas were also used to identify whether the position of the critical area differed between geometries studied, matching on particle size and velocity conditions, which individually are known to affect the critical area positions. Figure 4 also illustrates how the critical area position was affected by torso geometry. Consistent with the increased vertical velocity identified for the anatomical geometry, the critical area was *lower* for this geometry, compared to others, because this geometry had larger vertical velocity that caused particles to move upward with the freestream while moving toward the mouth. Table 4 summarizes the central locations of the critical areas, by geometry, particle size, and velocity condition. Over all velocities, the critical area positions were, on average, 17 mm higher for the full relative to the anatomical geometry and 30 mm higher for the truncated relative to the anatomical geometry. The location of the critical area for the truncated torso geometry at test conditions was always located higher than for the other geometries. The location of the critical area for the full model was always higher than for the anatomical torso,

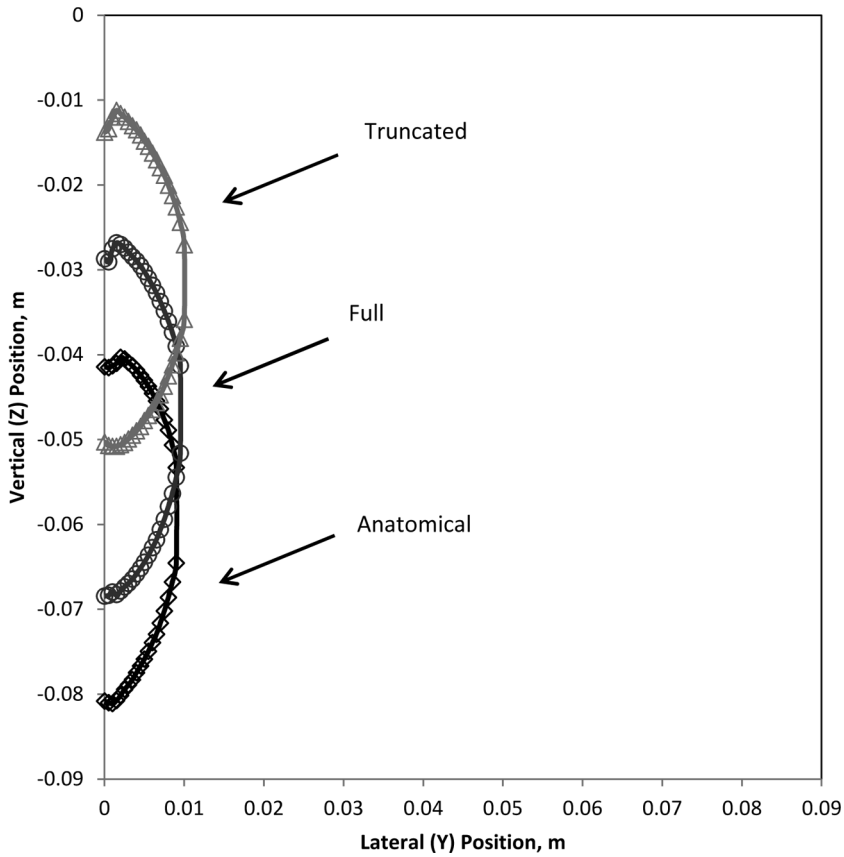

Fig. 4. Critical area for 7 µm particle in 0.4 m s^{-1} freestream velocity with at-rest breathing inhalation (1.81 m s^{-1}). Particles released 0.75 m upstream from mouth opening, centered at (X, Y, Z) = (0, 0, 0) m.

Table 4. Vertical position (Z) of critical-area midpoint. Center of mouth is positioned at $Z = 0$ mm.

Particle diameter (μm)	Freestream, breathing velocity ($m\ s^{-1}$)	Midpoint location (mm) for Torso geometry:		
		Truncated	Full	Anatomical
7	0.1, 1.81	−28.08	−52.02	−66.01
	0.1, 12.11	−27.32	−49.60	−69.80
	0.2, 1.81	−29.70	−46.57	−64.49
	0.2, 12.11	−30.40	−47.66	−66.54
	0.4, 1.81	−31.01	−47.64	−60.71
	0.4, 12.11	−32.15	−48.54	−63.89
22	0.1, 1.81	76.97	60.30	43.94
	0.1, 12.11	73.59	52.12	37.78
	0.2, 1.81	21.24	6.98	−10.77
	0.2, 12.11	20.49	4.24	−13.76
	0.4, 1.81	−5.00	−21.14	−33.84
	0.4, 12.11	−6.36	−22.32	−36.62
52	0.1, 1.81	578.89	569.19	558.43
	0.1, 12.11	554.49	549.75	287.17
	0.2, 1.81	281.59	270.38	258.13
	0.2, 12.11	278.03	264.87	252.53
	0.4, 1.81	127.63	113.16	103.56
	0.4, 12.11	124.95	111.52	98.76
68	0.1, 1.81	526.52	518.33	514.85
	0.1, 12.11	480.01	482.98	485.00
	0.2, 1.81	482.71	469.72	466.52
	0.2, 12.11	474.02	462.93	453.03
	0.4, 1.81	231.87	217.93	209.95
	0.4, 12.11	227.02	214.32	203.46
82	0.1, 1.81	723.74	711.01	707.27
	0.1, 12.11	673.18	664.95	660.61
	0.2, 1.81	375.93	366.89	359.90
	0.2, 12.11	356.39	347.93	341.54
	0.4, 1.81	183.90	172.05	166.72
	0.4, 12.11	178.99	168.96	160.15
100	0.1, 1.81	na	na	na
	0.1, 12.11	701.06	681.23	678.28
	0.2, 1.81	na	na	na
	0.2, 12.11	493.56	484.05	475.40
	0.4, 1.81	na	na	na
	0.4, 12.11	252.22	238.56	235.00
116	0.1, 1.81	na	na	na
	0.1, 12.11	620.00	602.37	604.44
	0.2, 1.81	na	na	na
	0.2, 12.11	632.02	623.69	618.03
	0.4, 1.81	na	na	na
	0.4, 12.11	322.25	311.41	306.06

na = For these conditions, no aspiration occurred for the indicated particle size.

which always had the lowest location. The difference between the locations of the critical areas between the three torso models decreased with increasing particle size, as gravitational settling dominates particle motion compared to the freestream. The difference in the location of the critical area was less pronounced for the heavy breathing conditions. These results show that torso geometry had a greater influence

on the location of the critical area for lower breathing rates. Although the location of the critical area changed with torso complexity, the size of the critical areas, by particle size and velocity conditions, were the same, regardless of torso complexity. The sizes of the critical areas were the same in matched velocity conditions because torso complexity did not affect lateral velocities, but only vertical velocities.

Aspiration efficiency

The computed aspiration efficiencies, by particle size, for each of the geometries and velocity condition tested are given in Table 5. For all torso models, the aspiration efficiency decreased with increasing particle size consistently for all velocity and breathing-rate conditions, as anticipated. For the heavy breathing rates, aspiration efficiency decreased from ~100% for the 7 µm particles to ~30% for 116 µm particles. For the at-rest breathing rates, aspiration efficiency dropped to 0% for particles larger than 82 µm, indicating that large particles were incapable of turning into the inhaling mouth. These trends were seen regardless of torso geometry. Aspiration efficiency estimates were larger over all particle sizes and breathing conditions for lower freestream velocities and decreased as freestream velocity increased.

This decreased aspiration for larger particles is similar to the behavior of the omni-directional ACGIH inhalable particulate mass (IPM) criterion curve. However, for larger particles, aspiration efficiency modeled here continued to decrease with increasing particle size whereas the IPM curve levels to 50% for particles larger than 50 µm. At-rest breathing rates (1.81 m s^{-1}) consistently had smaller mean aspiration efficiencies, with zero aspiration for particle sizes larger than 82 µm, significantly less than the 50% aspiration efficiency in the IPM sampling criterion. Aspiration efficiencies for the heavy breathing rate at all freestream velocities were larger for all three torso models compared to at-rest breathing.

Aspiration efficiency differences between the geometries, over all test conditions, ranged from −10.7 to 8.8% (Table 2). The anatomical torso aspiration efficiencies averaged 0.7% larger than the full cylinder torso but only 0.4% larger than the truncated torso. Paired, two-tailed *t*-tests identified statistically significant differences between the full and anatomical models ($P = 0.003$). The differences between the full and the truncated models, and the anatomical and truncated models were not statistically significant ($P = 0.115$ and 0.223, respectively). While differences in both vertical velocities and critical area positions varied between geometries, the resulting aspiration efficiencies were, at worst, ~10% different between geometries, and on average were 0.5% different over the range of estimates studied. The differences in aspiration efficiency estimates were relatively small, indicating that the use of a simplified truncated model would not substantially affect aspiration estimates in the range of indoor air velocities and the facing-the-wind orientation studied here.

DISCUSSION

The torso geometry resulted in significantly different velocity estimates in the chest and head regions. For this study, when velocity was examined separately for regions above the chin and regions of the neck and below, significant velocity differences ($P < 0.001$) were found in both regions between all torso models for all but one velocity and breathing rate condition between the anatomical and full models (0.2 m s^{-1}, at-rest breathing). Overall, the vertical

Table 5. Mean Aspiration efficiency (%) for all torso geometries.

Freestream velocity (m s^{-1})	Truncated						Full						Anatomical					
	0.1	0.1	0.2	0.2	0.4	0.4	0.1	0.1	0.2	0.2	0.4	0.4	0.1	0.1	0.2	0.2	0.4	0.4
Breathing rate (m s^{-1})	1.81	12.11	1.81	12.11	1.81	12.11	1.81	12.11	1.81	12.11	1.81	12.11	1.81	12.11	1.81	12.11	1.81	12.11
Particle size (µm)																		
7	100.8	100.6	98.4	99.4	98.2	103.0	100.9	99.9	97.6	99.4	98.1	98.6	100.9	100.1	97.9	99.0	97.6	98.8
22	99.4	99.7	97.3	98.0	97.6	104.3	99.2	99.7	97.7	98.2	97.5	98.1	99.3	99.7	96.9	98.3	96.8	98.2
52	87.0	94.0	85.8	93.3	79.7	97.1	86.9	94.8	86.4	93.0	81.7	91.6	86.9	94.1	83.5	93.1	83.5	92.2
68	70.8	89.8	61.8	89.0	56.4	84.5	72.2	89.8	63.1	88.7	57.5	78.2	72.3	90.0	69.9	89.7	58.9	83.2
82	21.6	82.7	21.1	84.7	28.2	73.3	23.9	82.9	22.9	84.8	30.1	68.7	24.9	72.0	26.0	87.3	34.3	74.9
100	0.0	69.5	0.0	48.2	0.0	50.5	0.0	71.3	0.0	49.7	0.0	47.5	0.0	69.1	0.0	56.9	0.0	51.7
116	0.0	22.8	0.0	26.2	0.0	34.2	0.0	23.6	0.0	27.1	0.0	32.7	0.0	22.5	0.0	28.6	0.0	35.1

velocity estimates ranged from 0.29 m s^{-1} to −0.21 m s^{-1}. Because the floor was closer to the breathing zone with the truncated geometry, the upward component of the vertical velocity near the torso was held to zero at hip height, whereas the taller cases allowed the velocity to develop an upward component over an additional meter in height, explaining the differences between the truncated and full torso models. The additional increase in vertical velocity for the anatomical versus full torso may be attributable to torso dimension differences: the bluff body associated with the female anatomical geometry was wider and it projected further upstream relative to the mouth (0.45137 m) compared to the cylindrical torso (0.1725 m deep).

The velocity findings from this study compare well with other non-inhaling studies that found larger velocity increases, relative to the freestream, in the chest region, but smaller velocity increases in the facial region. Smith and Bird (2002) found that velocity was decreased and reached a minimum in the chest region, but in the face region there was less deceleration of velocity. Topp *et al*. (2003) also noted velocity increases in the chest region but not as large increases in the head region. Thermal studies, although lacking inhalation, have also identified this trend. Those studies found that while *W* data at the chest height decreases with increasing model complexity, the ratio of the concentration in the mouth area to the concentration in the room did not.

The presence of legs has been found to influence velocity profiles as well. Topp *et al*. (2003) found that for seated mannequins, when legs were included in the model, the velocity at the center of the torso was significantly lower. Brohus and Nielsen (1996) found similar results that the inclusion of legs in the standing model caused a decrease in the upward vertical velocity in the region of the head. However, in this work, we found the full geometry had lower average vertical velocities for all breathing and freestream conditions over all regions when compared to the anatomical form with legs. When velocities below the neck region were examined, the full model still had lower velocities compared to the anatomical model. These results are different than the results seen in previous studies. This could be due in part because the anatomical model had a larger width than the full model (matched to underarm torso width, not shoulder width), whereas previous studies used models with and without legs with similar widths.

Using truncated or simplified torso geometry as a surrogate for the more complicated human torso was also associated with 14- to 30-mm shifts in the height of upstream locations where particles, if released, would be inhaled into the mouth of identically shaped faces. This trend is consistent with torso-induced vertical velocity differences. The location of the critical area moved downward as the torso complexity increased. Although these position differences were statistically significant, aspiration efficiency studies do not depend upon precise position information in aspiration calculations. Rather, aspiration efficiency determinations typically require the generation of a uniform particle concentration across the entire wind tunnel cross-section, including the relatively small critical areas.

While generally insignificant to aspiration estimation studies, this finding does identify a concern with the use of simplified torsos in 'other' CFD applications investigating human exposure. If using CFD techniques to examine exposures from a 'point' source or to validate a CFD model with wind tunnel data where contaminant concentrations are 'not' uniformly distributed, these differences in airflow based on simplifications to the human surrogate geometry may significantly affect the estimates of personal exposure from that point source. When Anthony and Flynn (2006a) attempted to compare particle transport from a nebulizer to an inhaling mannequin mouth between wind tunnel tests (small-scale anatomical mannequin) and CFD simulations (truncated, cylindrical torso), positional biases were considered. However, they attempted to resolve the differences between these systems by lowering the simulated aerosol source by only 5 mm of the experimental aerosol generators' positions, which was unsuccessful. As indicated by our study, this confirms that the velocity differences may have required repositioning the computational particle source even lower than the 5 mm attempted by these authors. Hence, torso simplifications are not recommended when contaminant transport from a specific reference location is required.

Anthony and Flynn (2006b) proposed that velocity differences associated with torso simplification (truncation, simple cylindrical shape) may have affected aspiration from a 50th percentile female CFD study, accounting for differences between their computational simulation results and Kennedy and Hinds (2002) wind tunnel experiments. They reported differences between computational and experimental aspiration efficiency estimates ranging from <10% for particles <52 µm to up to 40% for particles >68 µm. The −10.9 to 8.8% differences identified in this current study, as attributable to torso simplifications, are not sufficient to explain the differences between the computational and experimental results. Hence, the differences between CFD and

wind tunnel tests should not be attributed to torso simplifications.

The estimates of aspiration efficiency were found to decrease with increasing particle size for all velocity and breathing-rate conditions. This trend agreed with data published previously, although the aspiration estimates are larger than those found by both the previous studies by Anthony and Flynn (2006b) and Se *et al*. (2010).

This study concluded that the complexity of torso geometry had minimal effect on aspiration efficiency, even though the velocity and the position of critical areas were influenced by the torso geometry. The differences in aspiration efficiency by particle size and velocity condition were at most 8.8% and averaged between −0.3 and 0.7% over the test conditions studied here. The between-geometry differences were less important than the between breathing-rate aspiration efficiency estimates, where 4–35% differences were seen. Given the uncertainties and sampling error in experimental aerosol studies, these between-geometry differences are insufficient to account for differences between modeled and experimental results.

Although aspiration efficiencies were estimated for six discrete velocity conditions, realistically the conditions a worker encounters would vary across a wide range of velocities. Breathing velocities would vary from at-rest to heavy, and is not constant but rather cyclical, not represented here. Air movement around workers ranges from less than 0.1 m s^{-1} to larger than 0.4 m s^{-1}, particularly when a worker is moving or is near the supply or exhaust ventilation. To estimate the aspiration efficiencies a worker might experience during working conditions over a range of breathing conditions, aspiration efficiency for each torso was averaged for both breathing rates at 0.4 m s^{-1} and compared to facing the wind data from Kennedy and Hinds (2002), illustrated in Fig. 5. Aspiration efficiencies were larger for particles <68 µm for all three simulations compared to experimental aspiration efficiencies from Kennedy and Hinds (2002). However, for particles >68 µm, aspiration efficiencies were once again smaller than those reported experimentally. These results show that the truncation of the model in the computational studies is not enough to account for the differences between the computational and experimental aspiration efficiency estimates. The computational models still underestimate aspiration efficiencies compared to the experimental data. Anthony and Flynn also hypothesized that the differences between the computational and experimental aspiration estimates could be due to the different breathing patterns, and Kennedy and Hinds used cyclic breathing patterns with the peak inhalation higher than the average steady state used in the computational studies. The differences in the head and mouth dimensions could have contributed to the difference in results although the study by Anthony (2010) showed that facial features were not a large contributor to aspiration efficiency estimates. Particle bounce, especially for the larger particle sizes, may have also contributed

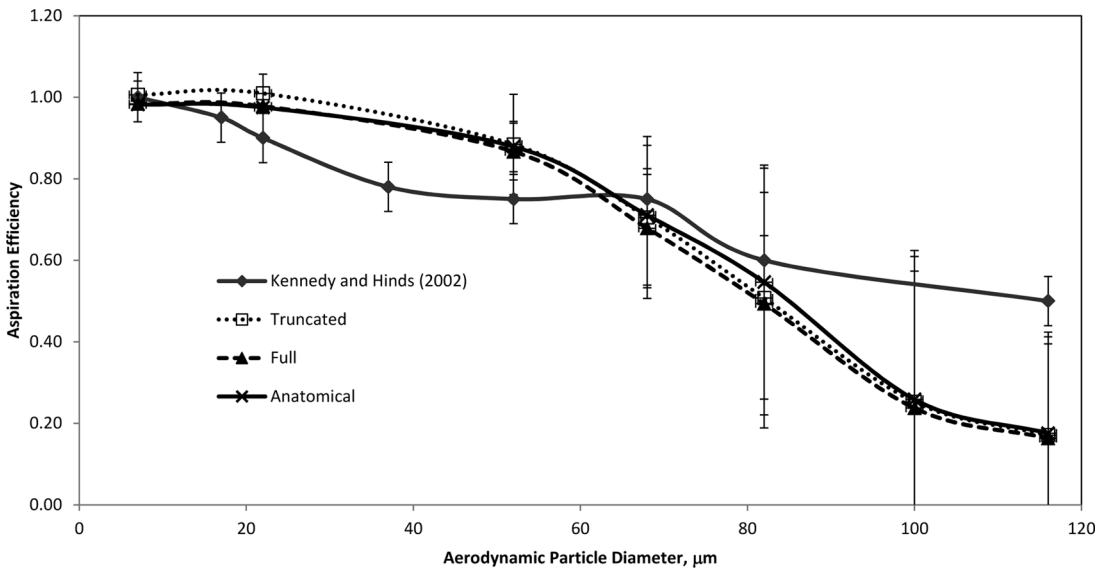

Fig. 5. Comparison of aspiration efficiency for truncated, full, and anatomical torso models to experimental data from Kennedy and Hinds (2002). Error bars represent one standard deviation.

to the differences. Laminar particle transport was used in the computational simulations providing mean estimates of aspiration: turbulent particle trajectory simulations may increase the mean estimates of particle aspiration computed in this work and may account for the differences seen. Additionally, incomplete particle discharging in Kennedy and Hinds (2002) experiment may have occurred, which could also contribute to the discrepancies seen between the experimental and computational results.

A major limitation of this study is that inhalation was simulated as constant, not cyclical breathing. Studies have shown that exhalation can play an important role in airflow patterns around the mouth. Exhalation, especially at heavy breathing rates, may have a more prominent influence on aspiration efficiency than torso complexity and should be investigated further.

Another limitation of this study is that it ignored thermal effects, which could play a large role on airflow patterns around the body, especially at the low velocities investigated in this study. Although airflow patterns around a body have been hypothesized to be influenced by thermal effects from the body, Aitken *et al*. (1999) did not find that aspiration efficiencies were influenced by the use of a heated mannequin. Further research is necessary to investigate the thermal effect on aspiration efficiency.

This study confirms that using a simplified torso is a reasonable approximation to complex human form for aspiration efficiency studies that require the assumption of uniform concentration of aerosol upstream of the inhaling humanoid form. However, this work was limited to the facing-the-wind orientation to investigate a rationale why previous modeling results may have differed from experimental studies. Not yet evaluated is whether this trend continues as the torso and inhaling mouth are rotated away from this orientation. While it has been hypothesized that the aspiration efficiency would decrease as the human faces away from the oncoming wind, the wake effects of the torso may be more significant with the back to the wind, and airflow through the legs may prove to be a more significant factor in both velocity field and particle trajectory modeling than they were in this simplified scenario. In addition, the standard *k*–epsilon turbulence model, used here, has problems estimating flow separation around objects, so future investigation with torso rotation should include additional turbulence models.

CONCLUSION

This research tested the hypothesis that torso simplifications in both shape and height can affect velocity, critical area location, and aspiration efficiency estimates. This study confirmed that vertical velocity and positions of critical areas were significantly different between torso geometries. However, comparisons of aspiration efficiency estimates between the simplified cylindrical, truncated torso and the fully anatomical torso yielded a maximum 8.8% difference, but averaged less than 1% over all velocity and particle sizes studied here. These differences are insignificant relative to between-velocity aspiration estimates. Specifically, when comparing at-rest to heavy breathing aspiration efficiency estimates, aspiration differences can be as large as 35%. The results from this study show that the use of the truncated model as a surrogate for a complex human form is appropriate for aspiration efficiency studies, although it is limited to facing the wind orientation. However, for studies investigating velocity flow or aspiration from a point source, a more realistic anthropometrically complex model is recommended, as truncation at the torso, both experimentally and computationally, would affect the particle trajectories of inhaled sources relative to a full-height human.

FUNDING

This research was supported by a grant from the National Institute for Occupational Safety and Health, Centers for Disease Control (R01OH009290). Its contents are solely the responsibility of the authors and do not necessarily represent the official views of NIOSH.

SUPPLEMENTARY MATERIAL

Supplementary material can be found at http://annhyg.oxfordjournals.org/.

REFERENCES

Aitken RJ, Baldwin PEJ, Beaumont GC *et al.*. (1999) Aerosol inhalablity in low air movement environments. J Aerosol Sci; 30: 613–26.

Anthony TR. (2010) Contribution of facial feature dimensions and velocity parameters on particle inhalability. Ann Occup Hyg; 54: 710–25.

Anthony TR, Flynn MR. (2006a) CFD model for a 3-D inhaling mannequin: verification and validation. Ann Occup Hyg; 50: 157–73.

Anthony TR, Flynn MR. (2006b) Computational fluid dynamics investigation of particle inhalability. J Aerosol Sci; 37: 750–65.

Anthony TR, Flynn MR, Eisner A. (2005) Evaluation of facial features on particle inhalation. Ann Occup Hyg; 49: 179–93.

Baldwin PEJ, Maynard AD. (1998) A survey of wind speeds in indoor workplaces. Ann Occup Hyg; 42: 303–13.

Brohus H, Nielsen PV. (1996) CFD models of persons evaluated by full scale wind channel experiments. Proceedings of Ventilation '97, The 5th International Symposium on Ventilation for Contamination Control, Global Developments in Industrial Ventilation, Ottawa, Canada, 14–17 September 1997. Vol 1. pp. 215–26.

Chung IP, Dunn-Rankin D. (1997) Experimental investigation of air flow around blunt aerosol samplers. J Aerosol Sci; 28: 289–305.

Ingham DB. (1981) The entrance of airborne particles into a blunt sampling head. J Aerosol Sci; 12: 541–49.

Kennedy NJ, Hinds WC. (2002) Inhalability of large solid particles. J Aerosol Sci; 33: 237–55.

Kennedy NJ, Tatyan K, Hinds WC. (2001) Comparison of a simplified and full-sized mannequin for the evaluation of inhalable sampler performance. Aerosol Sci Technol; 35: 564–68.

Maynard AD, Aitken RJ, Kenny LC *et al.* (1997) Preliminary investigation of aerosol inhalability at very low wind speeds. Ann Occup Hyg; 41 (Inhaled Particles VIII): 695–99.

Murakami S, Kato S, Zeng J. (2000) Combined simulation of airflow, radiation and moisture transport for heat release from a human body. Build Environ; 35: 489–500.

Ogden TL, Birkett JL. (1975) The human head as a dust sampler. In Halton WH, editor. Inhaled Particles IV: Proceedings of an International Symposium, Organized by the British Occupational Hygiene Society. Oxford: Pergamon Press. pp. 93–105. ISBN 0080205607.

Se CMK, Inthavong K, Tu J. (2010) Inhalability of micron particles through the nose and mouth. Inhal Toxicol; 22: 287–300.

Smith JP, Bird AJ. (2002) Relationship of sampling efficiency for manikin-mounted personal samplers to efficiency measurements made independent of manikin. J Aerosol Sci; 33: 1235–59.

Topp C, Hesselholt P, Trier MR *et al.* (2003) Influence of geometry of thermal manikins on concentration distribution and personal exposure. Proceedings of Healthy Buildings. Singapore.